Int. J. Electrochem. Sci., 15 **(2020)** 10243 – 10252, doi: 10.20964/2020.10.02

International Journal of
ELECTROCHEMICAL
SCIENCE
www.electrochemsci.org

Short Communication

Preparation of self-assembled N-Zn_2GeO_4 nanocomposite and their photocatalytic properties

Yanrong Lu, Riya Jin [*], Yina Qiao, Wenhui Liu, Kun Wang, Xiaojian Wang, Chaoqi Wang

School of Environment and Safety Engineering, North University of China, Taiyuan 030051, China
[*]E-mail: jrya@nuc.edu.cn

Received: 8 June 2020 / *Accepted:* 22 July 2020 / *Published:* 31 August 2020

In this study, a nanorod-like N-doped Zn_2GeO_4 was prepared by a simple single-pot solvothermal method without template. Characterization techniques like powder scanning electron microscopy (SEM), X-ray diffraction (XRD), X-ray photoelectron spectroscopy (XPS), UV-vis diffuse reflectance spectroscopy (DRS) were used. The N-doped Zn_2GeO_4 have good UV light absorption properties. N-doping introduces doped energy levels into the energy band structure of Zn_2GeO_4, thus improving the photocatalytic activity. Photocatalytic experiments showed that the degradation rate of rhodamine-B (RhB) with N-doped Zn_2GeO_4 (R_N=1) photocatalyst was nearly 95% within 3 min; 2.5 times higher than that pure Zn_2GeO_4 photocatalyst. Additionally, the N-doped Zn_2GeO_4 hierarchical photocatalyst have excellent chemical stability in the photocatalytic performance stability tests. Investigations indicated that the main active species involved in the photodegradation of RhB in N-doped Zn_2GeO_4 are the superoxide radical ($\cdot O_2^-$), while $\cdot OH$ and h^+ also play a role.

Keywords: Zn_2GeO_4; photocatalytic; N doping; Visible-light sensitization

1. INTRODUCTION

With rapid development of the economy, environmental problems arising from air pollution, solid waste pollution, and water pollution, have become increasingly prominent[1]. The printing and dyeing wastewater produced by the textile industry has become a difficult problem of environmental pollution because of its great changes in water quality, high content of organic matter, and the use of PVA slurries and additives. Printing and dyeing wastewater contains large quantities and many varieties of dyes; the most commonly used dyes are methylene blue, methyl orange, and rhodamine B. The molecular structure of these dyes contains benzene rings and acid groups, making them potentially carcinogenic substances. Conventional physical, chemical, and biological water treatment methods for such wastewater has low processing efficiency and is thus, extremely challenging[2]. Photocatalytic technology, for non-selective and effective oxidation of waste products, can be used to address this

challenge. The treatment process is simple, fast, and easy to operate and does not involve secondary pollution[3-6]. To run this process, the use of clean, renewable energy sources, like solar energy, can make this treatment even more eco-friendly.

Metal germanate is an important functional material with excellent properties in electricity, optics, and magnetism. Germanate compounds have attracted widespread attention in the fields of electrodes, humidity sensors, catalysis, ion exchange, adsorbed porous materials, and germanate glass as windows for high-energy laser systems[7-10]. Zn_2GeO_4 is one of the most notable germanates for its wide bandgap (4.68 eV) and outstanding photoelectric properties[7]. Due to the nanoscale effect and surface effect, Zn_2GeO_4 has fast photoelectric transmission properties and high sensitivity[7]. It is a fluorescent ceramic material with good optical properties. Zn_2GeO_4 demonstrates excellent photocatalytic performance and is well-known for decomposing water[11] and for degrading pollutant[12, 13].Recent research has been focused on improving the low photocatalytic activity of Zn_2GeO_4, and One of the main reasons is that the photocatalytic activity is not high enough to meet the actual demand. Studies indicate that the modification of Zn_2GeO_4 by ion doping, precious metal deposition and semiconductor composite is an effective method to improve the photocatalytic activity[11, 14-17]. Therefore, the modification of Zn_2GeO_4 by ion doping and the study of the optimal technological conditions for treatment of printing and dyeing wastewater are of great significance to the development of the textile industry, protection of human health, and environmental sustainability.

Here a nanorod-like and different doping concentrations N-doped Zn_2GeO_4 was prepared by a simple single-pot solvothermal method without template. The photocatalyst have been characterized by powder X-ray diffraction (XRD), scanning electron microscopy (SEM), X-ray photoelectron spectroscopy (XPS), and UV-vis diffuse reflectance spectroscopy (DRS) surface area measurements. N-doping introduced doped energy levels in the band structure of Zn, reducing the forbidden band width of Zn_2GeO_4, consequently making photo-induced electronic transitions easier. Studies prove that this ensures UV-light adsorption and high-performance photocatalysis for removal of a sample organic molecule, RhB. Since the catalytic activity mechanism of N-doping modified photocatalytic materials is not very clear, this study will provide new evidence for the explanation of N-doping mechanism.

2. EXPERIMENTAL SECTION

2.1. Preparation of N-doped Zn_2GeO_4 catalysts

N-doped Zn_2GeO_4 was prepared by improved solvothermal method. 0.52 g of GeO_2 and 3 g of $Zn(NO_3)_2{\cdot}6H_2O$ were first dissolved in 80 mL mixture of solvents [deionized water : diethanolamine (DEA) = 1:3] and stirred for 0.5 h. Then, we added a certain amount of urea to the mixture. R_x is defined as the atomic ratio of N to Ge, Here, and the value of R_N was set as 0, 0.5, 1.0, and 1.5. After stirring for 1 h, the mixture was transferred into a 100 mL autoclave with an inner Teflon5 lining and maintained at 170 °C for 24 h and then cooled to room temperature. The resulting white precipitate was collected by filtration and washed several times with deionized water and absolute ethanol before

drying the sample in an oven at 60 °C for 6 h, marked as Zn_2GeO_4, 0.5 N-Zn_2GeO_4, 1 N-Zn_2GeO_4, and 1.5 N-Zn_2GeO_4.

2.2. Material Characterization

Crystal structure analysis of N-doped Zn_2GeO_4. photocatalyst was carried out by the D/MaxRB XRD (Japan) with Cu Kα radiation from 5º-55º, with a scan rate of 0.02º s-1. The morphology of the samples was characterized by SEM (JSM-5610). XPS data were obtained using an ESCALab220i-XL electron spectrometer from VG Scientific using 300W AlKα radiation. Base pressure was about 3×10^{-9} mbar. The binding energies were referenced to the C1s line of amorphous carbon at 284.6 eV. The composition of the samples was studied by EDX (Inca Energy-200). The UV-vis diffuse reflectance spectra (UV-vis DRS) and UV-vis absorption spectra of the photocatalysts in the range of 200-700 nm was measured by UV-vis spectrometer.

2.3. Photocatalytic activity measurements

The photocatalytic degradation of rhodamine B (RhB) was carried out in a XPA photochemical reactor equipped with 1000 W high pressure mercury lamp. Use electric fans and cooling water to eliminate thermal effects. The photocatalytic activity of N-Zn_2GeO_4 and pure Zn_2GeO_4 were tested. 0.05 g photocatalyst was introduced into the Pyrex reactor, which was filled with RhB aqueous solution (10 $mg{\cdot}L^{-1}$) of 50 ml. Before light was turned on, the solution was stirred continuously in the dark for 30 min to ensure that the adsorption-desorption equilibrium was established. Take out an appropriate amount of suspension at regular intervals. Finally, the powder was removed by centrifuge and the supernatant was analyzed. The residual concentration of RhB was determined by spectrophotometer (UV9600, Beijing Ruili Instruments Co Ltd., China) at 553 nm. In order to determine the durability of the photocatalyst, the N-Zn_2GeO_4 nanocomposites were separated from the aqueous solution after each operation. The filtered solids are reused in subsequent recycling experiments without any treatment. The stability of the photocatalytic material was evaluated by repeating the above steps three times.

3. RESULTS AND DISCUSSION

The XRD patterns of the 1 N-Zn_2GeO_4 samples are shown in Fig.1. The predominant phase observed was orthorhombic (JCPDS file Card no. 85-0454, a=8.836 Å, b=8.836 Å and c=1.000 Å), with (110) as the preferred orientation, along with (221), (220), (120), (321), (131), (140), (431), (241), (511), (250), (523), (222), (541), (621), (360), and (150) reflections and none of the conventional impurities were detected[12]. No impure phases, such as GeO_2, were found, although GeO_2 appeared in other solution methods[18]. Thus, the N-doped Zn_2GeO_4 samples had good crystallinity and purity.

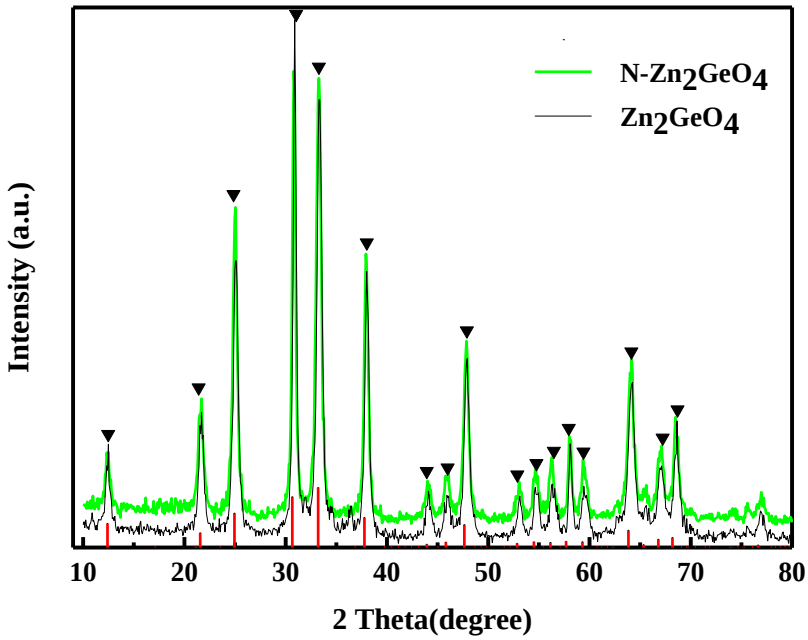

Figure 1. The XRD patterns of the as-prepared Zn_2GeO_4 and 1 N-Zn_2GeO_4 s samples

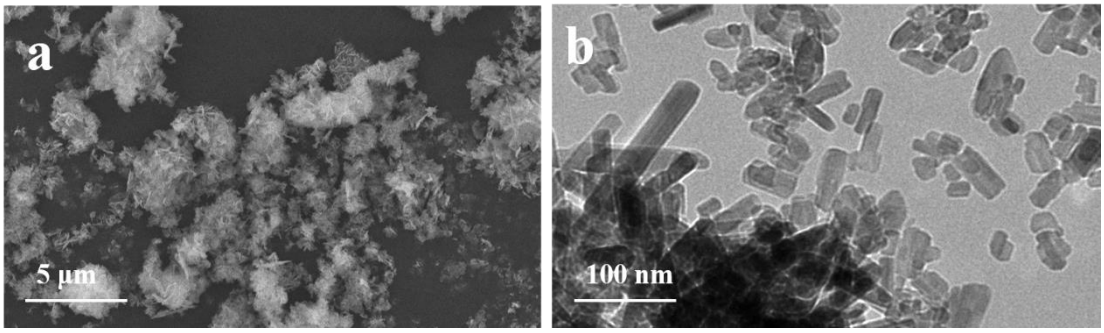

Figure 2. (a) The SEM images of N-Zn_2GeO_4 microflowers; (b) The TEM images of N-Zn_2GeO_4;

Fig. 2 shows the SEM and TEM images of N-Zn_2GeO_4 catalyst. From Fig. 2 (a), we can see that there are a large number of nanorods and obvious agglomeration, indicating that rod-like N-Zn_2GeO_4 photocatalytic materials were successfully prepared in this experiment. TEM images in Fig. 2 (b) show that at a higher magnification, N-doped Zn_2GeO_4 is composed of a mass of nanorods of different lengths.

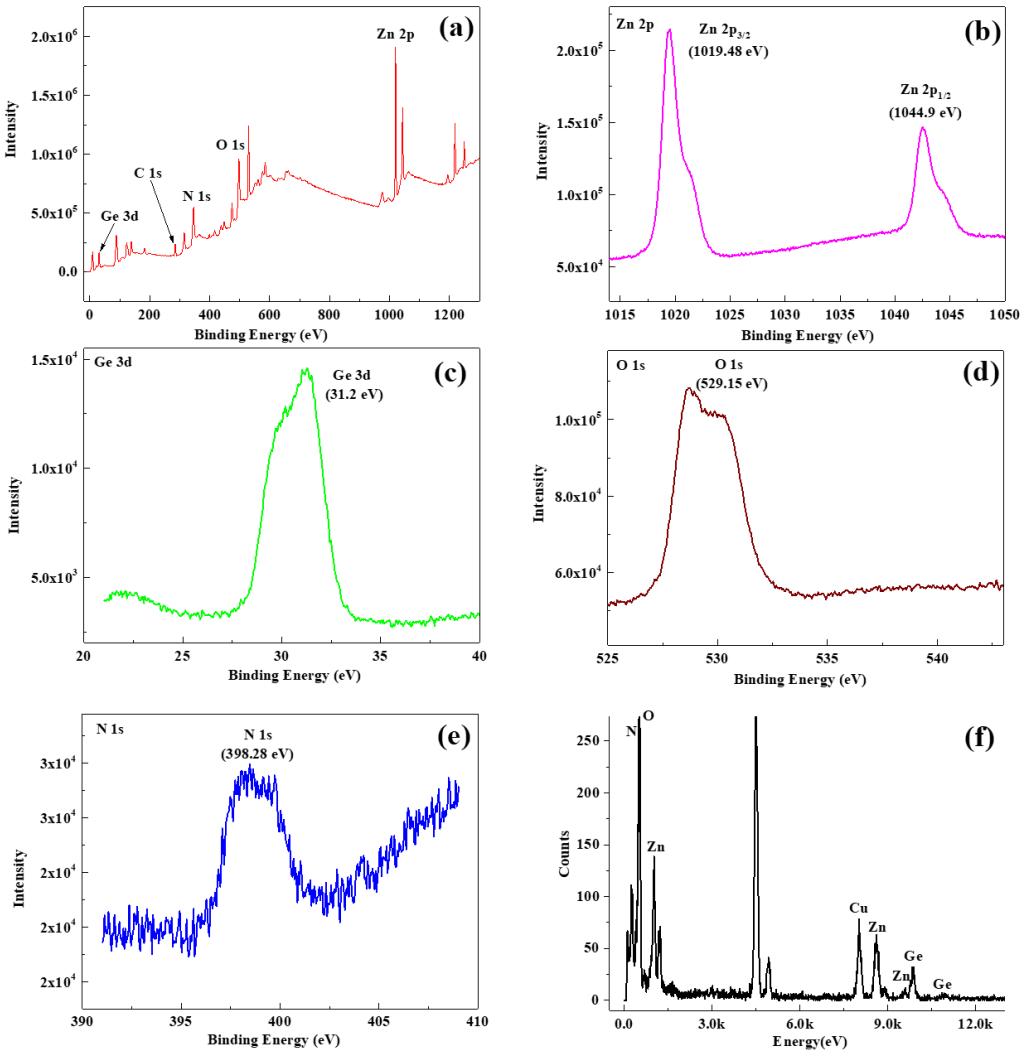

Figure 3. XPS spectra of N-doped Zn_2GeO_4: (a)survey spectrum, (b)Zn 2p, (c)Ge 3d, (d)O 1d, (e)N 1s; (f) EDX pattern of N-doped Zn_2GeO_4.

The chemical composition of 1 N-doped Zn_2GeO_4 was determined by XPS (Fig. 3). The determination process is to expose the sample to monochrome X-radiation and to evaluate the chemical state of the species on the sample surface. The binding energies obtained in XPS is standardized under 284.6eV with C as the reference material when the sample is charged.. According to the XPS survey (Fig. 3(a)), the sample contained only N, Zn, O, and Ge. The two strong peaks in the Zn 2p region at 1019.48 and 1044.9 eV indicate that Zn is in the Zn^{2+} oxidation state (Fig. 3(b))[11]. In the Ge 3d XPS spectrum (Fig. 3(c)), the peak at 31.2 eV reveals Ge is in its $[GeO_4]^{2-}$, *i.e.*, Ge^{6+} state[19]. Fig. 3(d) shows the high-resolution XPS spectra for the O 1s, and a peak is observed at 529.15 eV[20]. The XPS spectra of N 1s is shown in Fig. 3(e); the spectral peak corresponds to N 1s at 398.28 eV[21]. Furthermore, EDX also confirmed the existence of N in the catalyst (Fig. 3(f)). The atomic ratio of Zn to Ge was 1.9:1 and the atomic ratio of O to Ge was 3.3:1; proving that there are a large number of oxygen vacancy defects on the surface of the N-Zn_2GeO_4 catalysts[22]. The results

show that nitrogen-doped Zn_2GeO_4, with oxygen vacancy defects on the surface has been successfully prepared, which is consistent with the results of XRD and XPS analysis[21].

3.2. Photocatalytic performance

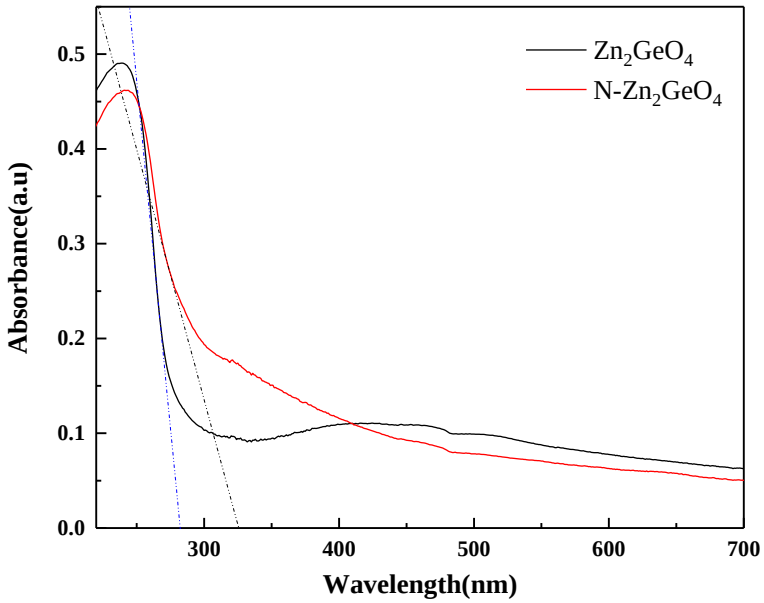

Figure 4. UV-Vis diffuse reflectance absorption spectra of Zn_2GeO_4 and 1 N-Zn_2GeO_4

The UV-visible diffuse reflectance absorption spectra of Zn_2GeO_4 and 1 N-Zn_2GeO_4 catalysts are shown in Fig. 4. The results show that both Zn_2GeO_4 and 1 N-Zn_2GeO_4 absorb light in the ultraviolet region. The absorption boundary of Zn_2GeO_4 and 1 N-Zn_2GeO_4 was calculated to be 282 nm and 325 nm, respectively. According to the formula, Eg=1240/λ, where Eg is bandgap energy and λ is absorption band-edge wavelength[23], the bandgap energy of Zn_2GeO_4 and 1 N-Zn_2GeO_4 can be calculated as 4.39 eV, and 3.35 eV, respectively. The curve for 1 N-Zn_2GeO_4 is redshifted in reference to that of pure Zn_2GeO_4, and N-doping reduces the forbidden bandwidth of Zn_2GeO_4, which is beneficial to the absorption of light and further improve the photocatalytic activity. This may be due to the introduction of doped energy levels in the band structure of Zn, making photo-induced electronic transitions easier[24].

The carrier transfer phenomena in N-Zn_2GeO_4 during the photocatalytic reaction was further studied. The valence band and conduction band potential of Zn_2GeO_4 were calculated as follows:

$$E_{CB} = X - Ee - 0.5Eg \quad (1)$$

$$E_{VB} = E_{CB} + Eg \quad (2)$$

where E_{CB} and E_{VB} are the conduction and valence band potentials of a semiconductor, respectively, X is the absolute negativity of semiconductor, Ee is the potential of free electrons relative to standard hydrogen electrodes (4.5 eV), and Eg is the band gap of a semiconductor. The results of the calculations from Equations are shown in Table 1.

Table 1. Electronegativity, Valence-band Potential, Conduction-band Potential and Bandgap Energy Zn_2GeO_4

	X	E_{CB} (eV)	E_{VB} (eV)	Eg (eV)
Zn_2GeO_4	6.04	-0.66	3.74	4.40

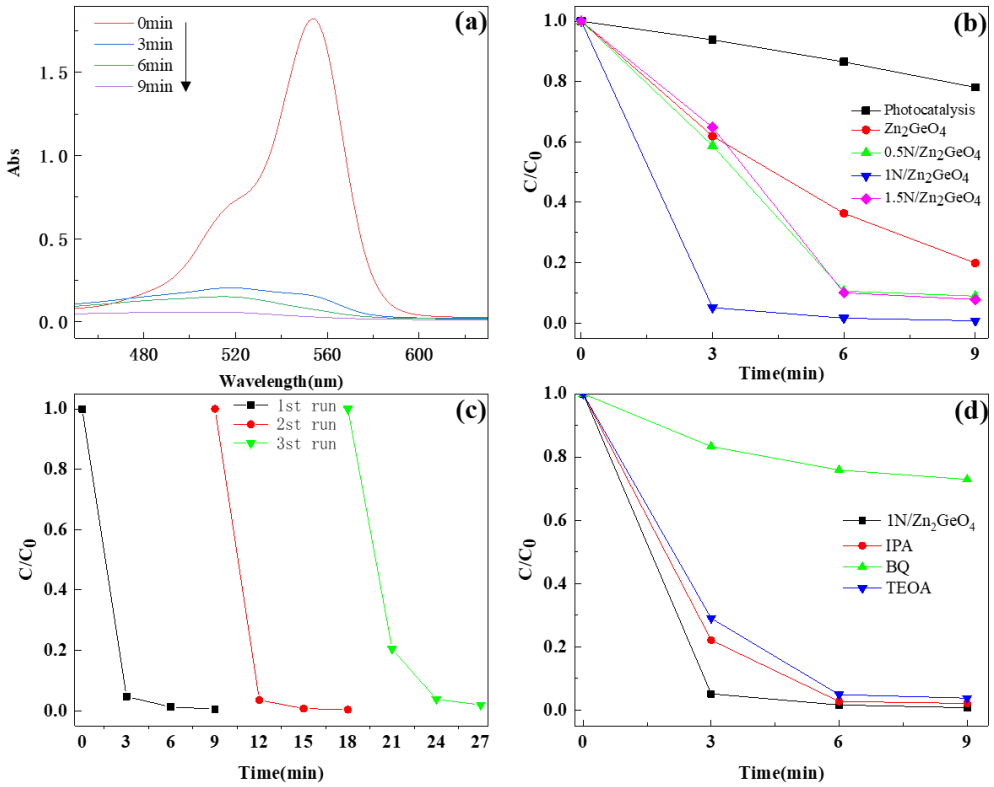

Figure 5. (a) UV light scanning pattern of 1-N-Zn_2GeO_4 degradation of RhB; (b) Effects of different catalysts on photocatalytic degradation of RhB under UV light; (c) Cycling runs of 1-N-Zn_2GeO_4 photocatalysts for the degradation of RhB; (d) Trapping experiments of active species during the photocatalytic reaction

In order to corroborate the photocatalytic activity of N-doped Zn_2GeO_4, an organic contaminant like RhB was selected for degradation. The catalysts with different R_N values (R_N=0, 0.5, 1, 1.5) were synthesized, and the degradation of RhB was carried out under UV light irradiation (Fig. 5(a)). The experimental results are grouped into two steps, *i.e.*, the adsorption process of pollutants on the surface of the photocatalyst, and the photodegradation process of the pollutants under UV irradiation. The depigmentation rate of RhB was promoted in the presence of pure Zn_2GeO_4 and N-doped Zn_2GeO_4 catalysts. It was found that nearly 95% of RhB degraded after 3 min for R_N = 1 while only 60% of RhB was eliminated with pure Zn_2GeO_4. The photocatalytic degradation rate of 1-N-doped Zn_2GeO_4 reached almost 100 % within 9 min, showing the best catalytic performance. However, an increase in N-doping did not enhance the depigmentation rate of RhB. Excessive N doping leads to the decrease of photocatalytic degradation rate in 3min. These results imply that modification by N-doping plays a

significant role in the photocatalytic process. Over doping will lead to agglomerations and hinder the surface active sites of the catalyst, resulting in low degradation rate.

Stability is an important aspect of commercialized photocatalytic materials. Fig. 5(c) shows three consecutive cycles of treatment of the RhB aqueous solution with 1-NZn_2GeO_4; it is evident that the degradation capacity was not significantly reduced. This shows that N-doped Zn_2GeO_4 photocatalytic materials are stable under UV light, and also have chemical stability.

By adding different active scavengers, the main oxidation species in the process of photocatalysis were investigated, and the mechanism of excellent photocatalytic performance of 1 N-Zn_2GeO_4 photocatalyst was obtained. Isopropyl alcohol (IPA), triethanolamine (TEOA), and 1,4-benzoquinone (BQ) were used as scavengers of ·OH, h^+ and $\cdot O_2^-$. After UV light illumination for 3 min, the decolorization rate of RhB was almost entirely suppressed on the addition of 1 mM BQ, while TEOA and IPA partially inhibited the decolorization rate of RhB (Fig. 5(d)). It can be inferred that the main active specie for photodegradation of RhB by N-doped Zn_2GeO_4 is the superoxide radical (O_2^-), while ·OH and h^+ also play a role.

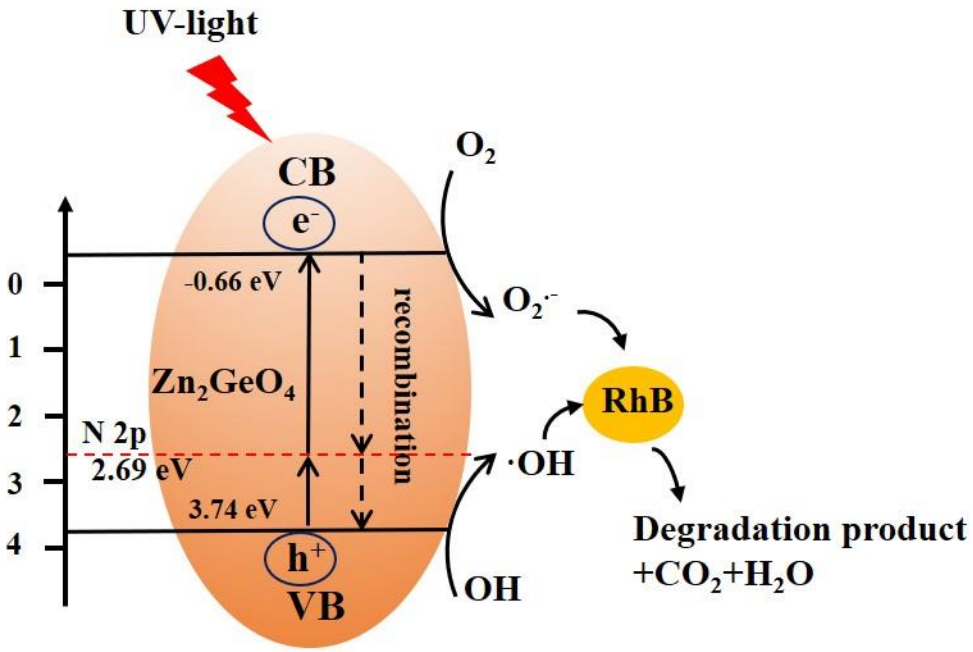

Figure 6. Schematic diagram of the photocatalytic mechanism of N-Zn_2GeO_4

According to the energy band structure of N-doped Zn_2GeO_4 photocatalyst and the experimental results of free radical capture, the possible diagram of photodegradation of RhB on N-doped Zn_2GeO_4 photocatalyst is given in Figure 6. UV irradiation can activate N-doped Zn_2GeO_4 photocatalyst to produce electron transition, forming oxidation hole (h^+) at the edge of valence band and reducing electron (e^-) at the edge of conductive band. The ultraviolet response of N-doped Zn_2GeO_4 results from the formation of intermediate energy levels slightly higher than the top of the Zn_2GeO_4 valence band, and the reduction of the hybrid band gap between N 2p and O 2p orbitals, which makes the electron transition between the Zn_2GeO_4 valence band and the conduction band easier, thus increasing the degradation rate of organic pollutants[25]. Subsequently, the electrons accumulated

in the Zn_2GeO_4 photocatalyst can capture the dissolved O_2 and induce it to form $\cdot O_2^-$. Organic pollutants can be further degraded by the oxidation of $\cdot O_2^-$ formed on the surface of the catalyst. At the same time, part of the holes in Zn_2GeO_4 on VB will react with some $OH^-$and H_2O to form hydroxyl (·OH), which has the ability to oxidize organic pollutant molecules. This is consistent with the above free radical capture experimental results. In the system of N-doped Zn_2GeO_4 photocatalytic degradation of RhB, the main active species are superoxide free radicals ($\cdot O_2^-$), while ·OH and h^+ also play a role in the photocatalytic degradation process. At the same time, due to the grating effect, over-doping reduces the amount of photons absorbed, thus reducing the apparent quantum efficiency of the photocatalytic process and the hole probability of interacting with the absorbed reactants on the surface of Zn_2GeO_4[26]. It is the main reason for the decrease of photocatalytic activity with the increase of R_N value.

4. CONCLUSIONS

In summary, the highly active, UV light-induced, N-doped Zn_2GeO_4 catalysts were prepared by a solvothermal method. The results of photodegradation of RhB by the catalysts indicated that N-doped Zn_2GeO_4 has high photocatalytic activity, and the photocatalytic performance had a significant relationship with the N-doping content. N doping can shorten the band gap and improve the catalytic activity. However, Over-doping reduces the amount of photons absorbed, thus reducing the apparent quantum efficiency of the photocatalytic process and the hole probability of interacting with the absorbed reactants on the surface of Zn_2GeO_4. The photocatalytic performance stability tests shows that the N-doping Zn_2GeO_4 hierarchical photocatalyst has excellent chemical stability. The $\cdot O_2^-$ were found to be the main active species in the presence of the N-doped Zn_2GeO_4 catalyst in aqueous solution, under UV light irradiation, rather than ·OH and h^+. This work provides new evidence for the explanation of the mechanism of N doping.

NOTES

The authors declare no competing financial interest.

ACKNOWLEDGMENTS

This work was supported by the Key Research and Development Projects of Shanxi Province (201803D31058).

References

1. R. Khan, A. Jabbar, I. Ahmad, W. Khan, A.N. Khan, J. Mirza, *Constr. Build. Mater.*, 30 (2012) 360-365.
2. L. Gonzalez-Gutierrez, C. Frontana, E. Martínez, A. *Cardenas-Robles, Procedia Chem.*, 12 (2014) 73-79.
3. N. Li, J. Liu, J.J. Liu, L.Z. Dong, Z.F. Xin, Y.L. Teng, Y.Q. Lan, *Angew Chem. Int. Ed. Engl.*, 58 (2019) 5226-5231.

4. S.K. Pahari, P. Pal, D.N. Srivastava, S. Ghosh, A.B. Panda, *Chem. Commun.*, 51 (2015) 10322-10325.
5. Y. Liu, L. Chen, Q. Yuan, J. He, C.T. Au, S.F. Yin, *Chem. Commun.*, 52 (2016) 1274-1277.
6. J. Hu, G. Xu, J. Wang, J. Lv, X. Zhang, Z. Zheng, T. Xie, Y. Wu, *New J. Chem.*, 38 (2014) 4913-4921.
7. M.M. Jumidali, K.M. Sulieman, M.R. Hashim, Structural, *Appl. Surf. Sci.*, 257 (2011) 4890-4895.
8. H.W. Kim, H.G. Na, J.C. Yang, C. Lee, *Chem. Eng. J.*, 171 (2011) 1439-1445.
9. L. Lu, J. Chen, W. Wang, *Appl. Phys. Lett.*, 103 (2013) 123902.
10. M. Yang, X.-q. Jin, *J. Cent. South Univ.*, 21 (2014) 2837-2842.
11. X. Li, Y. Feng, M. Li, W. Li, H. Wei, D. Song, *Adv. Funct. Mater.*, 25 (2015) 6858-6866.
12. L. Zhang, X.-F. Cao, Y.-L. Ma, X.-T. Chen, Z.-L. Xue, *Cryst. Eng. Comm.*, 12 (2010) 3201.
13. Q. Liu, Y. Zhou, Z. Tian, X. Chen, J. Gao, Z. Zou, *J. Mater. Chem.*, 22 (2012) 2033-2038.
14. L. Sun, Y. Qi, C.J. Jia, Z. Jin, W. Fan, *Nanoscale*, 6 (2014) 2649-2659.
15. G. Jiang, B. Tang, X. Li, Z. Wei, X. Wang, W. Chen, J. Wan, L. Shen, *Powder Technol.*, 251 (2014) 37-40.
16. Q. Zhang, K. Pang, Y. Xu, *J. Am. Ceram. Soc.*, 101 (2018) 5858-5869.
17. T. Yan, T. Wu, Y. Zhang, M. Sun, X. Wang, Q. Wei, B. Du, *J. Colloid Interface Sci.*, 506 (2017) 197-206.
18. B. Ma, F. Wen, H. Jiang, J. Yang, P. Ying, C. Li, *Catal. Lett.*, 134 (2010) 78-86.
19. Z.Q. Li, X.S. Lin, L. Zhang, X.T. Chen, Z.L. Xue, *Mater. Res. Bull.*, 47 (2012) p.2422-2427.
20. J. Liang, Y. Cao, H. Lin, Z. Zhang, C. Huang, X. Wang, *Inorg. Chem.*, 52 (2013) 6916-6922.
21. S. Sato, R. Nakamura, S. Abe, *Appl. Catal.*, 284 (2005) 131-137.
22. W. Liu, R. Jin, L. Hu, H. Zhong, L. Ren, S. Hu, *J. Mater. Sci. - Mater. Electron.*, 30 (2019) 10912-10922.
23. H. Fu, C. pan, W. Yao, Y. Zhu, *J. Phys. Chem.B*, 109 (2005) 22432-22439.
24. B. Tang, G. Jiang, Z. Wei, X. Li, X. Wang, T. Jiang, W. Chen, J. Wan, *Acta Metall. Sinica*, 27 (2014) 124-130.
25. R. Nakamura, T. Tanaka, Y. Nakato, *J. Phys. Chem. B*, 108 (2004) 10617-10620.
26. M. Miyauchi, A. Ikezawa, H. Tobimatsu, H. Irie, K. Hashimoto, *Phys. Chem. chem. Phys.*, 6 (2004) 865